Available online at www.sciencedirect.com
ScienceDirect
European Journal of Pharmaceutics and Biopharmaceutics 66 (2007) 466–474
European Journal of Pharmaceutics and Biopharmaceutics
www.elsevier.com/locate/ejpb

Research paper

Influence of sample characteristics on quantification of carbamazepine hydrate formation by X-ray powder diffraction and Raman spectroscopy

F. Tian [a], F. Zhang [a], N. Sandler [a], K.C. Gordon [b], C.M. McGoverin [b], C.J. Strachan [c], D.J. Saville [a], T. Rades [a,*]

[a] School of Pharmacy, University of Otago, Dunedin, New Zealand
[b] Department of Chemistry, University of Otago, Dunedin, New Zealand
[c] Drug Discovery and Development Technology Centre (DDTC), University of Helsinki, Finland

Received 15 October 2006; accepted in revised form 7 December 2006
Available online 13 December 2006

Abstract

This study aimed to assess the suitability of two widely utilized solid state characterization techniques namely powder X-ray diffraction (XRPD) and Raman spectroscopy, in polymorph detection and quantification for carbamazepine anhydrate and dihydrate mixtures. The influences of particle size, particle morphology, mixing, and in particular, surface bias on quantitation were investigated. Binary mixtures of carbamazepine anhydrate (form III) and dihydrate were prepared and analyzed using both XRPD and Raman spectroscopy in combination with partial least squares analysis. It was found that in principle both XRPD and Raman spectroscopy could be used to build calibration models for quantitative analysis, and a satisfactory correlation between the two techniques could be achieved. However, Raman spectroscopy appeared to be a more reliable quantification method because problems such as different particle size, morphology, and special distribution of the two solid state forms of the drug seemed to have no significant influence on Raman scattering in this study. The robust nature of Raman analysis greatly facilitates the whole quantification process from the preparation of calibration models to the quantification of *in situ* CBZ–DH conversion.

Keywords: Raman spectroscopy; X-ray powder diffraction; Carbamazepine; Carbamazepine dihydrate; Quantification

1. Introduction

The identification and quantitative characterization of crystalline forms of pharmaceutical materials are recognized as critical issues in the development of new drug products. There is a growing awareness of the significant influence of polymorphic and pseudopolymorphic transitions on the physico-chemical properties and pharmaceutical performance of drug products [1,2]. Carbamazepine (CBZ) is a typical example demonstrating the importance of polymorphism and pseudopolymorphism. CBZ has been routinely used for the treatment of epilepsy for over 20 years, however, CBZ has a low therapeutic index [3]. Six different CBZ polymorphs and pseudopolymorphs have been identified each with different physico-chemical properties [4–7]. Consequently, CBZ is an ideal candidate for attempting to establish relationships between polymorphic structures and properties, such as solubility/bioavailability characteristics or physical/chemical stability. The CBZ system also serves as an excellent model to study how analytical techniques perform in solid-state analyses.

There are a number of solid-state characterization techniques, classified by Brittain (1995) [8], based on the level at

* Corresponding author. School of Pharmacy, University of Otago, P.O. Box 913, Dunedin, New Zealand. Tel.: +64 3 479 5410; fax: +64 3 479 7034.
E-mail address: thomas.rades@stonebow.otago.ac.nz (T. Rades).

0939-6411/$ - see front matter © 2006 Elsevier B.V. All rights reserved.
doi:10.1016/j.ejpb.2006.12.002

which they probe solid-state properties; ranging from molecular to particulate and bulk techniques. Techniques at the particulate level include X-ray powder diffraction (XRPD), optical and electron microscopy, and thermal methods such as differential scanning calorimetry (DSC). Among these, XRPD is a widely employed analytical technique for both qualitative and quantitative characterization purposes of crystalline drugs, and its use in this context has been reported in many papers [9–11]. However, it has been pointed out that X-rays in a typical XRPD experimental setup only have a small mean penetration depth (~30 μm for Cu Kα radiation) [12] which implies that only a thin sample layer is analyzed in the Bragg-Brentano $\theta/2\theta$ geometry which may lead to poor particle statistics [13]. Also a range of sample properties such as particle size, packing, and sample thickness are known to affect the observed X-ray diffraction data [9,14,15].

Vibrational spectroscopies, such as Raman and IR spectroscopy probe solid-state properties at the molecular level. These techniques have been applied in polymorphic investigations [16,17]. The information obtained using Raman and IR spectroscopy may be complementary; however, Raman spectroscopy can offer some unique advantages over IR which facilitates its application in polymorphic investigations [18,19]. For instance, Raman spectroscopy only requires simple sample preparation, the scattering signal from water is low, and glass and plastic sample cells can be used [20,21]. Raman spectroscopy might also be used to identify compounds especially in complex mixtures, as the Raman spectra often have fewer and sharper features compared with the respective IR spectra [22]. The influence of surface scattering on the Raman signal has been widely reported and can significantly affect the outcome of the analysis [23,24]. Also, sub-sampling has been reported to be a problem with quantitative Raman spectroscopy [25–27]. Although no defined solution of sub-sampling has been established, it was found that several methods could greatly improve the measurements for instance employing large spot non-contact optics [28], moving the sample or excitation beam during data acquisition, and also employing multivariate analysis for data evaluation [29]. Furthermore, two commonly known limitations of Raman measurements are sample fluorescence and sample degradation, which however can be avoided in most cases by shifting the excitation wavelength to the NIR spectral region [30].

In the present study, the CBZ (form III) compacts were exposed to water, which led to the formation of DH during exposure predominantly at the surface of the compact as found from an earlier study [31]. Calibration models formed from binary mixtures of CBZ and DH (calibration samples) were built to quantify the amount of DH formation on the compacts (compact samples) during exposure to water. The aim of this study was to investigate the influence of properties of calibration samples and compact samples in polymorph quantification using XRPD and Raman methods. Partial least square (PLS) modeling, known to be more robust to experimental variations than traditional univariate analysis [32], was used to compare XRPD and Raman spectroscopy based CBZ polymorph quantification. A specific purpose of this study was to investigate whether there is a surface bias using these two techniques and if so, whether this leads to significant impairment in the performance of quantitative analyses.

2. Materials and methods

2.1. Materials

CBZ form III (Scientific Supplies Ltd., Auckland, NZ) was ground in an oscillatory ball mill (Mixer Mill MM301, Retsch GmbH & Co., Germany) for 5 min, and this reduced the size of the examined particles to ⩽5 μm. XRPD was used to confirm that the polymorphic form of CBZ remained unchanged after ball milling and that no significant amount of amorphous CBZ was formed.

Carbamazepine dihydrate (DH) was prepared from CBZ by recrystallization from an ethanol–water mixture as reported by Krahn and Mielck [6]. The yield DH was sieved to the size range of 180–250 μm (Test sieves, Endecotts Ltd., England). DH in the size range of ⩽5 μm was produced using the same method as described above. XRPD was again used to confirm that DH remained unchanged after ball milling.

2.2. Methods

2.2.1. Preparation of calibration samples

Binary mixtures of CBZ and DH were prepared at 20% (w/w) intervals from 0 to 100% CBZ in DH (200 mg per sample) using geometric mixing. Every mixture was prepared in triplicate, and every sample was measured in triplicate.

2.2.2. Preparation of compact samples

CBZ (200 mg) in the size range of ⩽5 μm was weighed and compressed into flat-faced compacts (12 mm in diameter and 2 mm thickness) using a hydraulic press (Model 3392, Freds. Carver Inc., USA) at a pressure of 70 MPa. Compacts were held at this pressure for 20 s. XPRD was used to confirm that the polymorphic form of CBZ (form III) remained unchanged after compression and that no amorphous CBZ was formed.

2.2.3. Exposure of compact samples to water

A six-station dissolution apparatus (D800 dissolution tester, Logan Instrument Corp.) with 200 ml distilled water was used. The CBZ compacts were placed at the bottom of the dissolution vessels without stirring at room temperature, and recovered after predetermined periods of 20, 40, 60, 1440, 2880, and 4320 min. CBZ compacts were exposed to water in triplicate for each time interval. The excess water on the compact samples was gently adsorbed using a tissue and samples were then measured both intact and

ground into a powder by XRPD and Raman immediately after recovery. Morphology of the DH growing on the surface of compact samples was examined using SEM (see below). For quantitative measurements, it was assumed that the dissolution of CBZ or the formed DH had a negligible influence on the proportion of the two solid-state form of the drug in the compact samples since both CBZ and the formed DH are only very slightly soluble in water at room temperature [33]. All compact samples were prepared in triplicate, and every sample was measured in triplicate.

2.2.4. X-ray powder diffraction (XRPD)

XRPD was performed using a PANalytical X'Pert PRO MPD system (PW3040/60) (PANalytical B.V., The Netherlands) with Cu Kα radiation ($\lambda = 1.542$ Å) and a divergence slit of 1°. The X-ray generator was set to an acceleration voltage of 30 kV and a filament emission of 40 mA. Samples were scanned between 3° (2θ) and 40° (2θ) using a step size of 0.008° (2θ) and a count time of 2 s. Data were collected using X'Pert Data Collector and viewed using X'Pert Data Viewer (PANalytical B.V., The Netherlands). The intact compact samples were placed directly on a flat aluminum sample holder. The powdered compact samples were packed into a standard aluminum sample holder and measured in the same way as the calibration samples.

2.2.5. Raman spectroscopy

The FT-Raman instrument consisted of a Bruker FRA 106/S FT-Raman accessory (Bruker Optik, Ettlingen, Germany) with a Coherent Compass 1064-500N laser (Coherent Inc, Santa Clara, USA) attached to a Bruker IFS 55 FT-IR interferometer, and a D 418-T Ge diode detector. Analysis was carried out at room temperature with a laser wavelength of 1064 nm (Nd:YAG laser) and a laser power of 120 mW. Back-scattered radiation was collected at an angle of 180°. The diameter of the laser beam at focus was approximately 300 μm according to the instrument manufacturer. Calibration samples were measured in aluminum cups, and intact compact samples were measured by placing them directly facing the Raman laser. The powdered compact samples were measured in the same way as the calibration samples. A total of 64 scans was averaged for each sample over a range from 3500 cm^{-1} to (−1000) cm^{-1} at a resolution of 4 cm^{-1}. Sulfur was used as reference standard to monitor the wavenumber accuracy. OPUS™ 5.0 (Bruker Optik, Ettlingen, Germany) was used for all spectral analyses.

2.2.6. Scanning electron microscopy (SEM)

For consistency, the surface of the compact samples facing the top of the dissolution pot was chosen for SEM investigation. The excess liquid was removed from the compacts as described above and samples were then immediately mounted onto a strip of double-sided carbon tape and sputter coated with a thin layer of gold–palladium under argon vacuum prior to SEM analysis. SEM micrographs were also taken of dry intact CBZ and DH compacts, and CBZ and DH powder samples. SEM imaging was performed using a Cambridge Instrument, Stereoscan 360, at 15 kV acceleration voltage. Micrographs were recorded using a PGTE Mitsubishi video/copy processor.

2.2.7. Thermogravimetric analysis (TGA)

The weight loss of the compact sample recovered after exposure to water for 4320 min was measured using a TGA – Q50 (TA instruments, New Castle, USA). The excess liquid was removed from the test sample as described above, and the sample (approximately 5 mg) was then powdered and transferred onto the platinum sample pan. The sampling was carried out in triplicate. The heating range used was from 25 to 210 °C at a heating rate of 10 °C/min using dry nitrogen as a purge gas. The total volatile yield was calculated from the mass loss in the TGA – Q50.

2.2.8. Multivariate analysis

Multivariate analysis was performed using the Quant2 package that accompanies OPUS™ software (Bruker Optics, Germany). The selection of spectral (or diffraction) regions for calibration was based on the wavenumber (or diffraction angle) regions that showed the largest differences between the components and therefore provided the greatest contribution to the linear regression equation for the analyte. All spectra (or diffractograms) were mean centered. The calibration models were calculated using the PLS algorithm and cross-validation (one sample removed per cycle). The root-mean-squared errors of cross-validation (RMSECV) were determined for each number of factors.

2.2.9. Statistical tests

Differences in the quantified values from XRPD and Raman were tested by one-way analysis of variance (ANOVA) and Tukey's pairwise comparisons (significance level was 0.05) using Minitab 12.1 software (Minitab Ltd., USA).

3. Results and discussion

3.1. Particle size and morphology of calibration samples

Particle size and morphology can greatly influence the exposed surface area of crystals and affect the mixing process in the preparation of a calibration curve. This may directly affect the linearity of the concentration–response profile when building a calibration curve [34]. The pure components of the calibration samples used (CBZ and DH) were therefore examined by SEM. The micrographs taken for the pure CBZ and DH samples having different sizes are shown in Fig. 1.

Morphology differences between CBZ and DH were clearly apparent in the micrographs of samples with a

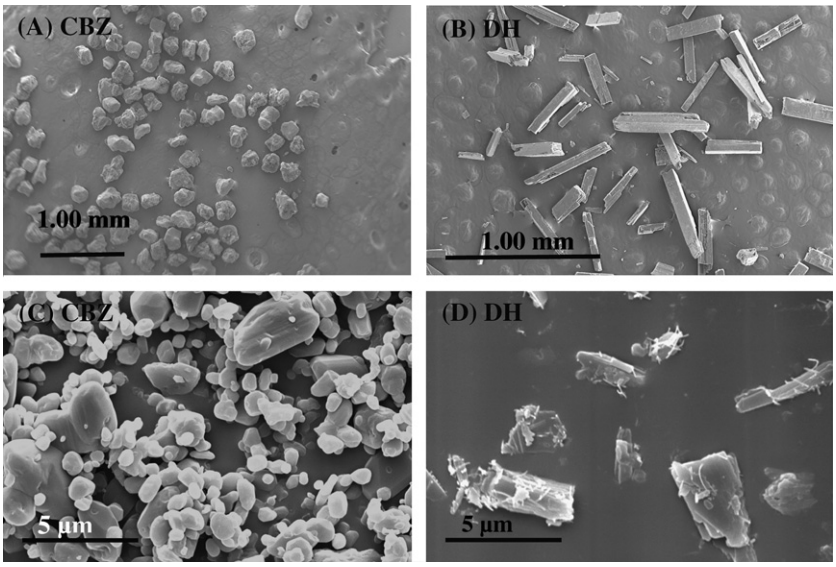

Fig. 1. SEM micrographs of CBZ and DH in two size ranges: 180–250 μm (A and B); ⩽5 μm (C and D).

particle size of 180–250 μm (Fig. 1A and B). CBZ was present as prism like crystals whereas DH was present as short needle-like crystals. The particle size of CBZ and DH crystals was dramatically reduced after grinding, and was mostly ⩽5 μm (Fig. 1C and D), but differences in morphology between the two solid-state forms of the drug remained.

3.2. Particle size and morphology of compact samples

The morphology of grown DH on the surface of compacts is shown in Fig. 2.

The DH concentration on the surface of the compact samples increased with increasing exposure time. However, the morphology of DH grown on the surface of test samples is different from the DH morphology of the calibration samples (shown in Fig. 1B and D). The DH formed during exposure to water was initially present as highly elongated thin needles that aggregated in the first 60 min (Fig. 2A–C), and became more densely packed after a longer exposure period of 1440 min (Fig. 2D–F).

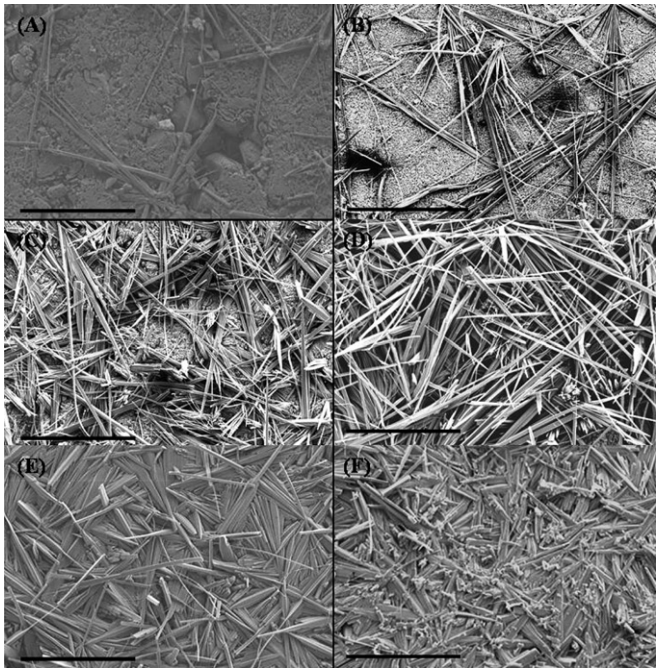

Fig. 2. The morphology of DH growth on the surface of test samples observed by SEM. The test samples were recovered after exposure to water for 20 min (A), 40 min (B), 60 min (C), 1440 min (D), 2880 min (E), and 4320 min (f). All photographs were taken using the same magnification, bars: 200 μm.

3.3. Calibration models built using XRPD and Raman spectroscopy

Following the International Conference on Harmonization, accuracy is defined as the closeness of agreement between the reference value and the value predicted from the calibration model [35]. In order to achieve a high accuracy of the quantitative analysis, various calibration models were built such that the calibration samples had properties that closely agreed with those of the compact samples. Firstly, the grown DH needles in the compact samples appeared to be highly exposed on the surface (Fig. 2). This situation is obviously different from the situation in the calibration samples where DH needles were well mixed with CBZ. Therefore, the compact samples were measured both intact (with DH on top of the surface) and ground up (with DH mixed with CBZ). Secondly, the DH on the surface of the compact samples was of large crystal size. One calibration model was therefore built from mixtures of fine form III (⩽5 μm) and large size DH (180–250 μm) particles.

The parameters used in generating the calibration models and also the linearity of the models are listed in Table 1.

Table 1
Parameters used in the generation of the quantitative models

Calibration curve	Form III (⩽5 μm) DH (180–250 μm)		Form III (⩽5 μm) DH (⩽5 μm)	
	XRPD	Raman	XRPD	Raman
Pre-processing	Multiplicative scattering correction (MSC)			
Regions used	5–30° (2θ)	3300–2900 cm^{-1} 1800–400 cm^{-1}	5–30° (2θ)	3300–2900 cm^{-1} 1800–400 cm^{-1}
Factors used	2	2	2	2
RMSECV (%)	14.0	2.75	2.93	1.06
R^2	0.832	0.994	0.993	0.999

The model prepared using 180–250 μm DH crystals and ⩽5μm CBZ showed very poor linearity when using XRPD (RMSECV was 14.0 and R^2 was 0.832) (Table 1).

There are several potential problems with XRPD when the large crystal size DH (180–250 μm) was used, which could have caused the poor performance of this calibration model. Firstly, DH needles are elongated while the form III powder consists of prism like crystals with relatively smooth surfaces. Blending was therefore difficult as the two solid-state forms of the drug differ in size and morphology. Although efforts were made to uniformly blend the DH and CBZ in the calibration samples, the mixtures appeared to be inhomogeneous. The same problem was also recently reported in a quantitative study carried out by Kipouros et al. [34].

Secondly, the maximum acceptable particle sizes of CBZ and DH in quantitative XRPD have been calculated according to Brindley's equation [36] and are 15.4 and 14.1 μm, respectively [9]. The X-ray absorption process may be unsatisfactory when particles larger than the ideal sizes are used.

Thirdly, some degree of preferred orientation has been detected by comparing the XRPD obtained from the sample when the sample was rotated by 90°. This can hardly be avoided in these samples if the large needle-like crystals of DH with size of 180–250 μm are present. It has also been reported that preferred orientation could be completely overcome only if some comprehensive treatment in both the experimental and the analytical approaches were used for instance performing a three-dimensional rotation of a capillary sample holder, employing a two-dimensional detector [37,38]. This however is not a conventional diffraction geometry and was unavailable in this study.

Fourthly, microabsorption can also be a potential problem. Microabsorption is known to stem from differences in the interactions of each material with the X-ray radiation. Microabsorption could be a serious problem when a powder mixture has constituents with very different particle size [39], as is the case in this calibration model. Lastly, in addition to the possible problems listed above, a large particle size can also induce primary extinction, leading to an obvious decrease in the diffraction intensity when crystalline samples used are large in size and/or have a high degree of imperfection [9].

On the other hand, the calibration model built using the same large DH/small CBZ particle samples showed reasonably good linearity when Raman spectroscopy was used (RMSECV (%) was as small as 2.75 and R^2 was 0.994). Although there have been some reports concerning the influence of particle size on Raman calibration [40,41], it has also been found that the effect can be suppressed under certain conditions such as employing proper spectral correction procedures [42]. In this study, sample properties, especially particle size, had no significant effect on the calibration model obtained from the Raman data, and this was further confirmed by the quantitative studies on compact samples presented below.

The calibration models improved greatly when samples with very fine particle sizes (⩽5 μm) were used, especially for XRPD, where high linearity in the concentration-response features was obtained as indicated by low values of RMSECV (<3.00) and high values of R^2(>0.990) (Table 1). The calibration models were shown to be physically meaningful by examination of the loading plots. For both the XRPD and Raman calibration models the first factor loading plots reflected the spectral differences between CBZ and DH. Therefore, these two calibration curves were used for quantitative analyses of compact samples presented in the following section.

3.4. Characterization of the compact samples using XRPD and Raman

3.4.1. XRPD

Fig. 3 shows the XRPD diffractograms for the initial and also recovered intact compact samples after exposure to water.

The characteristic DH peaks at 8.8° (2θ) and 12.2° (2θ) appeared after 20 min, but were very small (Fig. 3B). With increasing exposure time, the DH peaks became more prominent (Fig. 3C–G). In contrast, the characteristic peaks of CBZ became smaller with increasing exposure time (Fig. 3B–D), and only a very small peak at 13.0° (2θ) could be seen after 1440 min exposure (Fig. 3E). This peak was not present at 2880 or 4320 min (Fig. 3F–G).

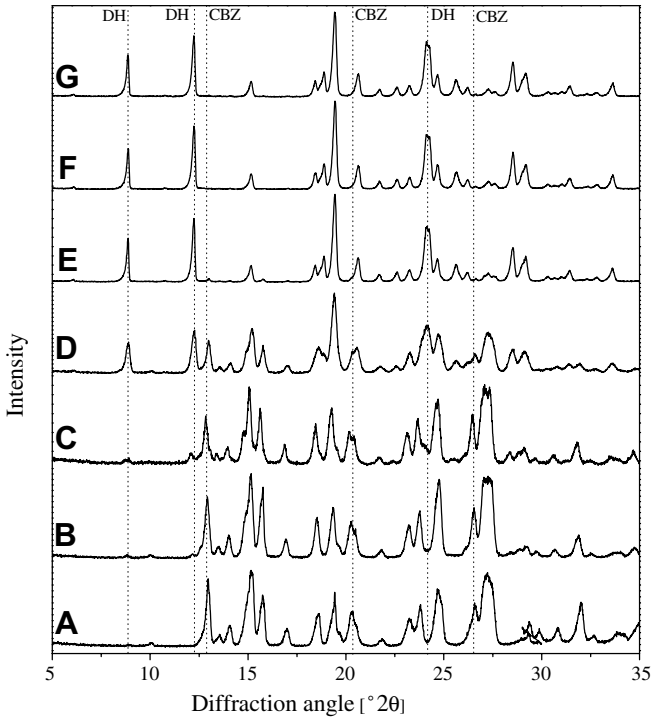

Fig. 3. XPRD diffractogram of initial compact sample (A), and of recovered intact compact samples after exposure to water for 20 min (B), 40 min (C), 60 min (D), 1440 min (E), 2880 min (F), and 4320 min (G).

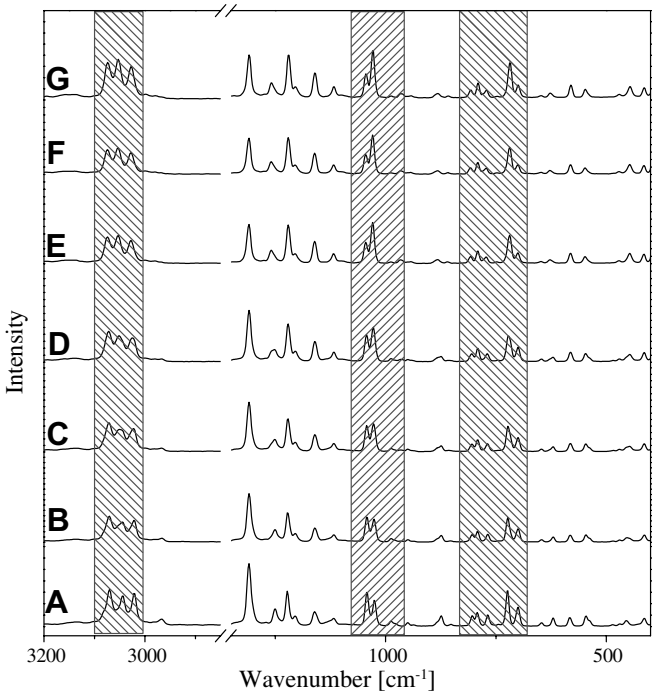

Fig. 4. Raman spectra of initial compact sample (A) and recovered intact compact samples after exposure to water for 20 min (B), 40 min (C), 60 min (D), 1440 min (E), 2880 min (F), and 4320 min (G). Areas showing the most obvious differences between CBZ and DH are shaded.

3.4.2. Raman spectroscopy

Fig. 4 shows Raman spectra for the initial and also recovered intact compact samples after exposure to water.

The Raman spectra of the recovered compacts also showed an increasing trend of DH formation with increasing exposure time to the water (Fig. 4). This agreed well with the XRPD diffractograms.

3.5. Quantification of the compact samples

The formation of DH in the compact samples was quantified for both intact and ground into powder samples using XRPD and Raman spectroscopy as shown in Fig. 5.

Using Raman spectroscopy (Fig. 5), there was no significant difference in the quantified DH amount between intact and powdered compact samples at all time points ($P > 0.05$). This showed that there was a good penetration of the Raman laser into the sample. For XRPD, significant differences between intact and powdered compact samples were seen for the first two time points (20 and 40 min) ($P < 0.05$), but with increasing formation of DH on the test sample, the predicted values became similar ($P > 0.05$). One plausible explanation for this difference could be the penetration problem of the X-ray beam as described in Section 1. The higher predicted amount of DH from the intact compact samples than from the powdered ones might be due to its higher exposure to the X-ray beam when orientated on the surface of the sample instead of being well mixed in a powdered one, which then leads to an over-represented signal in XRPD.

There was a significant difference in the predicted values between Raman and XRPD methods ($P < 0.05$). The percent weight loss of the compact sample recovered after 4320 min exposure was measured by TGA. The value obtained was $13.52\% \pm 0.07$ (w/w) (mean $\pm$ SD, $n = 3$). This is in excellent agreement with the theoretical water content in pure DH (13.2% (w/w)) [10]. Therefore, TGA

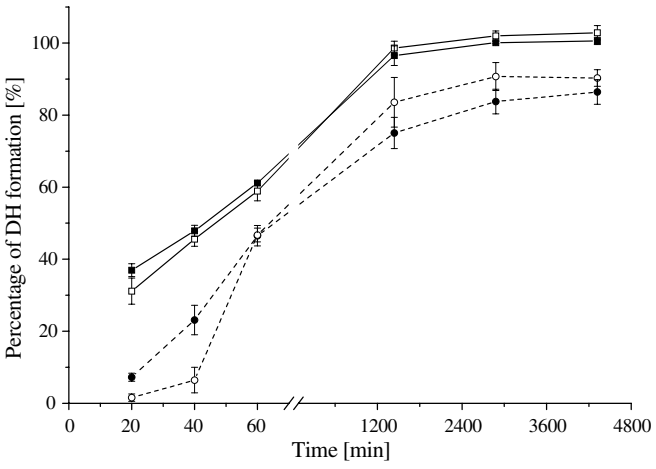

Fig. 5. The formation of DH on compact samples during exposure to water as a function of exposure time quantified by XRPD (in dashed lines; intact compacts (●) and powdered compacts (○)) and Raman spectroscopy (in solid lines; intact compacts (■) and powdered compacts (□)).

confirmed that the compact sample had totally converted to the DH, and thus supported the value obtained from Raman spectroscopy and indicated an under-prediction in XRPD.

As described above, the morphology and particle size of DH grown on the surface of the compact samples is different from that of DH of the calibration samples, where also problems such as preferred orientation are likely to be induced in the X-ray diffractrogram of needle-like DH samples. Therefore, for a deeper understanding of the under-prediction in XRPD, the compact samples recovered after a long exposure of 4320 min measured both intact and powdered are plotted together with calibration DH samples of the two different particle size ranges (Fig. 6).

The diffractograms were almost identical for the compact samples measured either intact or ground into a powder (Fig. 6C and D). However, obvious peak pattern differences in the diffractograms between DH grown from the compact samples and the DH calibration samples could be observed, especially in the shaded areas (19.2–19.9° (2θ) and 23.9–25.0° (2θ)). Also, the X-ray patterns between the calibration DH samples of two different particle sizes (Fig. 6A and B) were different at 8.9° (2θ) and 12.4° (2θ) and also in the shaded areas. Therefore, it should be noted that crystal size itself in this study could influence the relative peak intensities in the XPRD measurements. Although it is hard to determine the exact reasons for the differences in the relative peak intensities between the DH samples used in the calibration models and the compact samples, particle size and morphology differences could both be possible explanations, where problems as preferred orientation might contribute to the different relative peak intensities.

For a better comparison, Raman spectra of these samples were also checked. In contrast to the diffractograms described above, the Raman spectra were very consistent among all the DH samples (Fig. 7), regardless of calibration or compact samples.

To improve the accuracy of the calibration model for the compact samples, the specific diffraction angles' range of 19.2–19.9° (2θ) and 23.9–25.0° (2θ) in the XRPD diffractograms was excluded from building the calibration curve, and the parameters used in generating the new calibration model are listed below in Table 2. The predicted values for compact samples from this new calibration curve are plotted together with those gained from Raman spectroscopy for a clearer comparison (Fig. 8).

The values predicted from XRPD for the last three time points (1440–4320 min) greatly increased and became not significantly different from those obtained by Raman spectroscopy ($P > 0.05$). However, the values obtained in the initial 60 min were still significantly different from those determined by Raman spectroscopy ($P < 0.05$).

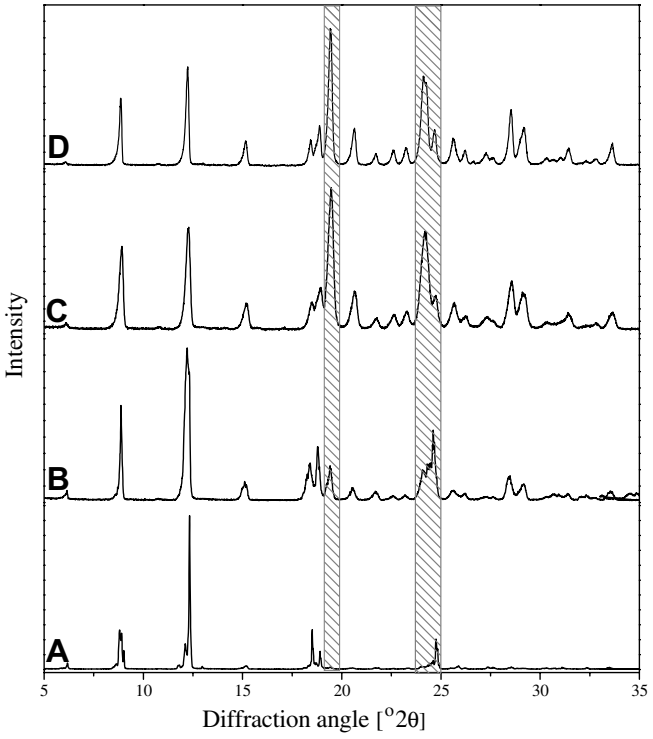

Fig. 6. XRPD diffractograms of pure DH calibration samples in size range of 180–250 μm (A) and ⩽5 μm (B), and the compact samples recovered after a long exposure of 4320 min (powdered (C) and intact (D)). Areas showing particularly obvious differences in the diffractograms between calibration and compact samples are shaded.

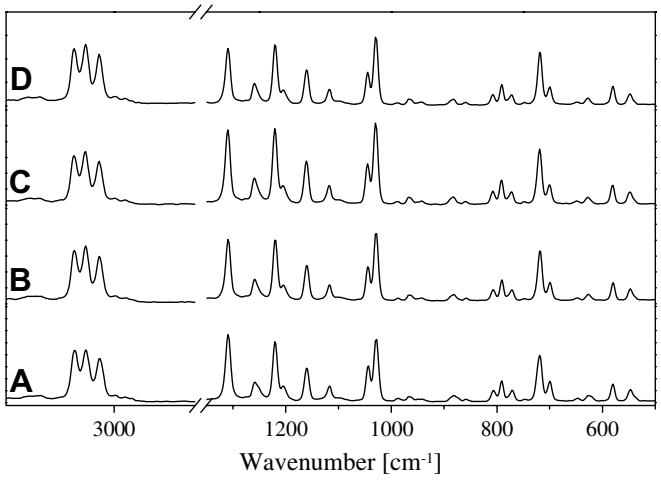

Fig. 7. Raman spectra of pure DH calibration samples in size range of 180–250 μm (A) and ⩽5 μm (B), the compact samples were recovered after a long exposure time of 4320 min (powder (C) and intact (D)).

Table 2
Parameters used in the generation of the quantitative models

Calibration curve	Pre-processing	Regions used	Factors used	RMSECV (%)	R^2
Form III (⩽5 μm) DH (⩽5 μm)	MSC	5.0–19.2° (2θ) 19.9–23.9° (2θ) 25.5–30.0° (2θ)	2	3.04	0.990

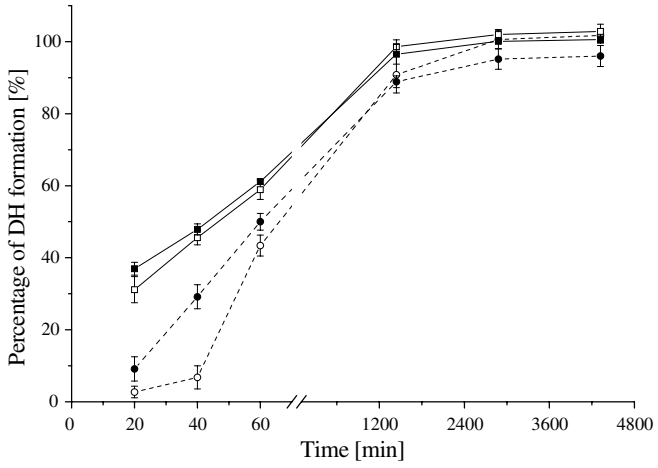

Fig. 8. The formation of DH on the CBZ compacts during exposure to water as a function of exposure time quantified by new calibration model in XRPD (in dashed lines; intact compacts (●) and powdered compacts (○)) and Raman spectroscopy (in solid lines; intact compacts (■) and powdered compacts (□)).

4. Conclusions

It is shown in the present study that both XRPD and Raman spectroscopy combined with PLS could in principle be used to evaluate the polymorphic conversion of CBZ compacts to the DH. However, Raman spectroscopy appeared to be a more reliable quantification method because problems such as different particle size, morphology, and spatial distribution of the two solid-state forms of the drug seemed to have no significant influence on Raman scattering in this study. The robust nature of Raman analysis greatly facilitates the whole quantification process from the preparation of calibration models to the quantification of *in situ* CBZ–DH conversion.

References

[1] S. Byrn, R. Pfeiffer, M. Ganey, C. Hoiberg, G. Poochikian, Pharmaceutical solids: a strategic approach to regulatory considerations, Pharm. Res. 12 (1995) 945–954.
[2] Guidance for Industry. PAT – a framework for innovative pharmaceutical manufacturing and quality assurance, U.S. Food and Drug Administration (FDA), Rockville, MD, USA, 2004, 21.
[3] M.C. Meyer, A.B. Straughn, J.J. Eric, G.C. Wood, F.R. Pelsor, V.P. Shah, The bioinequivalence of carbamazepine tablets with a history of clinic failures, Pharm. Res. 9 (1992) 1612–1616.
[4] V.L. Himes, A.D. Mighell, W.H. De Camp, Structure of carbamazepine: 5H-Dibenz[*b,f*]azepine-5-carboxamide, Acta Crystallogr. B37 (1981) 2245–2248.
[5] A.L. Grzesiak, M.D. Lang, K. Kim, A.J. Matzger, Comparison of the four anhydrous polymorphs of carbamazepine and the crystal structure of form I, J. Pharm. Sci. 92 (2003) 2260–2271.
[6] F.U. Krahn, J.B. Mielck, Effect of type and extent of crystalline order on chemical and physical stability of carbamazepine, Int. J. Pharm. 53 (1989) 25–34.
[7] G. Reck, G. Dietz, The order-disorder structure of carbamazepine dihydrate: 5H-dibenz[*b,f*]azepine-5-carboxamide dihydrate, C15H12N2O, Cryst. Res. Technol. 21 (1986) 1463–1468.
[8] H.G. Brittain (Ed.), Physical characterization of pharmaceutical solids, Marcel Dekker, Inc., New York, USA, 1995, p. 1.
[9] R. Suryanarayanan, Determination of the relative amounts of anhydrous carbamazepine (C15H12N2O) and carbamazepine dihydrate (C15H12N2O. 2H2O) in a mixture by powder X-ray diffractometry, Pharm. Res. 6 (1989) 1017–1024.
[10] J. Han, R. Suryanarayanan, Influence of environmental conditions on the kinetics and mechanism of dehydration of carbamazepine dihydrate, Pharm. Dev. Technol. 3 (1998) 587–596.
[11] W.W.L. Yong, R. Suryanarayanan, Kinetics of transition of anhydrous carbamazepine to carbamazepine dihydrate in aqueous suspensions, J. Pharm. Sci. 80 (1991) 496–500.
[12] Á.G. De La Torre, A. Cabeza, A. Calvente, S. Bruque, M.A.G. Aranda, Full phase analysis of Portland Clinker by penetrating synchrotron powder diffraction, Anal. Chem. 73 (2001) 151–156.
[13] D.L. Kaiser, J.R.L. Watters, Certificate of Analysis; Standard Reference Material 1878a, National Institute of Standards and Technology, Gaithersburg, MD 20899, 2005, 1–4.
[14] R. Suryanarayanan, Determination of the relative amounts of a-carbamazepine and b-carbamazepine in a mixture by powder X-ray diffractometry, Powder Diffr. 5 (1990) 155–159.
[15] R. Suryanarayanan, X-ray powder diffractometry, in: H.G. Brittain (Ed.), Physical Characterization of Pharmaceutical Solids, Marcel Dekker, New York, USA, 1995, pp. 187–222.
[16] F. Tian, J.A. Zeitler, C.J. Strachan, D. Saville, C.K. Gordon, T. Rades, Characterizing the conversion kinetics of carbamazepine polymorphs to the dihydrate in aqueous suspension using Raman spectroscopy, J. Pharm. Biomed. Anal. 40 (2006) 271–280.
[17] C. Strachan, D. Pratiwi, K.C. Gordon, T. Rades, Quantitative analysis of polymorphic mixtures of carbamazepine by Raman spectroscopy and principal components analysis, J. Raman Spectrosc. 35 (2004) 347–352.
[18] A.C. Williams, Some pharmaceutical application of Raman spectroscopy, in: I.R. Lewis, H.G.M. Edwards (Eds.), Handbook of Raman Spectroscopy: From the Research Laboratory to the Process Line, Marcel Dekker, Inc., New York, USA, 2001, p. 575.
[19] H. Wikström, P.J. Marsac, L.S. Taylor, In-line monitoring of hydrate formation during wet granulation using Raman spectroscopy, J. Pharm. Sci. 94 (2005) 209–219.
[20] P.A. Anquetil, C.J.H. Brenan, C. Marcolli, I.W. Hunter, Laser Raman spectroscopic analysis of polymorphic forms in microliter fluid volumes, J. Pharm. Sci. 92 (2002) 149–160.
[21] S.N. Campbell Roberts, A.C. Williams, I.M. Grimsey, S.W. Booth, Quantitative analysis of mannitol polymorphs, FT-Raman spectroscopy, J. Pharm. Biomed. Anal. 28 (2002) 1135–1147.
[22] S. Webster, K.J. Baldwin, Raman spectroscopy for pharma. Part II: Raman as a PAT tool, Pharma. Technol. Eur. 17 (2005) 30–35.
[23] B.O. Sullivan, P. Barrett, G. Hsiao, A. Carr, B. Glennon, In situ monitoring of polymorphic transitions, Org. Process Res. Dev. 7 (2003) 977–982.
[24] H. Wang, C.K. Mann, T.J. Vickers, Effect of powder properties on the intensity of Raman scattering by crystalline solids, Appl. Spectrosc. 56 (2002) 1538–1544.
[25] C.M. Deeley, R.A. Spragg, T.L. Threlfall, A comparison of Fourier transform infrared and near-infrared Fourier transform Raman spectroscopy for quantitative measurements: an application in polymorphism, Spectrochim. Acta, Part A: Mol. Biomol. Spectrosc. 47A (1991) 1217–1223.
[26] F.W. Langkilde, J. Sjoblom, L. Tekenbergs-Hjelte, J. Mrak, Quantitative FT-Raman analysis of two crystal forms of a pharmaceutical compound, J. Pharm. Biomed. Anal. 15 (1997) 687–696.
[27] L.S. Taylor, G. Zografi, The quantitative analysis of crystallinity using FT-Raman spectroscopy, Pharm. Res. 15 (1998) 755–761.
[28] H. Wikström, I.R. Lewis, L.S. Taylor, Comparison of sampling techniques for in-line monitoring using Raman spectroscopy, Appl. Spectrosc. 59 (2005) 934–941.
[29] J. Johansson, S. Pettersson, S. Folestad, Characterization of different laser irradiation methods for quantitative Raman tablet assessment, J. Pharm. Biomed. Anal. 39 (2005) 510–516.

[30] D.E. Bugay, Characterization of the solid state: spectroscopic techniques, Adv. Drug Deliv. Rev. 48 (2001) 43–65.
[31] F. Tian, N. Sandler, J. Aaltonen, C. Lang, D.J. Saville, K.C. Gordon, C.J. Strachan, J. Rantanen, T. Rades, Influence of polymorphic form, morphology and excipient interactions on the dissolution of carbamazepine compacts, J. Pharm. Sci. in press.
[32] R.J. Hendershot, R. Vijay, B.J. Feist, C.M. Snively, J. Lauterbach, Multivariate and univariate analysis of infrared imaging data for high-throughput studies of NH3 decomposition and NOx storage and reduction catalysts, Meas. Sci. Technol. 16 (2005) 302–308.
[33] M. Windholz, The Merck Index, 10th ed., Merck, Rahway, NJ, 1983, 246.
[34] K. Kipouros, K. Kachrimanis, I. Nikolakakis, V. Tserki, S. Malamataris, Simultaneous quantification of carbamazepine crystal forms in ternary mixtures (I, III, and IV) by diffuse reflectance FTIR spectroscopy (DRIFTS) and multivariate calibration, J. Pharm. Sci. 95 (2006) 2419–2431.
[35] International Conference on Harmonization, ICH Harmonised Tripartite Guideline-Validation of analytical procedures: Method. Fed Regist, 62 (1997), 27463.
[36] G.M. Brindley, The X-ray identification and crystal structures of clay minerals, in: G. Brown (Ed.), Mineralogical Society, London, 1961, p. 492.
[37] P. Bergese, E. Bontempi, I. Colombo, L.E. Depero, Micro X-ray diffraction on capillary powder samples: a novel and effective technique for overcoming preferred orientation, J. Appl. Crystallogr. 34 (2001) 663–665.
[38] N.S. Murthy, R.J. Barton, Industrial Application of X-ray Diffraction, in: H.F. Chung, D.K. Smith (Eds.), Marcel Dekker, New York, USA, 2001, pp. 495–507.
[39] B.M. Pederson, R.M. Gonzalez, R.S. Winburn, Minimization of microabsorption effects in complex mixtures, International Center for Diffraction Data, Adv. X-ray Anal. 46 (2003) 68–73.
[40] J. Schöll, D. Bonalumi, L. Vicum, M. Mazzotti, M. Müller, In situ monitoring and modeling of the solvent-mediated polymorphic transformation of L-glutamic acid, Cryst. Growth Des. 6 (2006) 881–891.
[41] S.E.J. Bell, J.R. Beattie, J.J. Mcgarvey, K.L. Peters, N.M.S. Sirimuthu, S.J. Speers, Development of sampling methods for Raman analysis of solid dosage forms of therapeutic and illicit drugs, J. Raman Spectrosc. 35 (2004) 409–417.
[42] H. Qu, M. Louhi-Kultanen, J. Rantanen, J. Kallas, Solvent-mediated phase transformation kinetics of an anhydrate/hydrate system, Cryst. Growth Des. 6 (2006) 2053–2060.